SLAC – PUB – 4046
August 1986
(T/E)

Perturbative QCD Predictions for Inclusive Production of Heavy Mesons in e^+e^- Annihilation*

CHUENG-RYONG JI†

Stanford Linear Accelerator Center
Stanford University, Stanford, California, 94305

and

Institute of Theoretical Physics, Department of Physics,
Stanford University, Stanford, California 94305

and

FARHANG AMIRI*

Stanford Linear Accelerator Center
Stanford University, Stanford, California, 94305

ABSTRACT

Perturbative quantum chromodynamic predictions are given for inclusive production of heavy mesons, D, B and T, at energy range of 20-110 GeV. At high energy limit, analytic calculations of total cross sections, fragmentation functions, and angular distributions are presented. For T mesons, higher twist mass effects are included in numerical estimates. We found these effects give 20%-30% corrections for D and B meson productions at $\sqrt{s} \sim 60$ GeV. The forward-backward asymmetry from weak-electromagnetic interference is found to be large at TRISTAN energy.

Submitted to *Physical Review D*

---

* Work supported by the Department of Energy, contract DE – AC03 – 76SF00515.
† Present address: Department of Physics, Brooklyn College, Brooklyn, NY 11210.
Work supported by the National Science Foundation, grant PHY–85–08735.
* Permanent address: Physics Department, Weber State College, Ogden, UT 84408.
Work supported by the Department of Energy, contract DE–AC07–76ET10723.

1. Introduction

The present vigorous experimental programs at the existing accelerators and at the ones under construction are expected to subject quantum chromodynamics (QCD) and electroweak theory to ever more stringent tests. Specifically, e^+e^- colliders at center of mass energies of $\sqrt{s} \sim 100$ GeV will provide the opportunity to explore many of the predictions of QCD and electroweak theory in a clean environment and therefore they are ideal testing grounds within their energy ranges.

In e^+e^- annihilations, the interaction is mediated by electromagnetic current (γ) and the weak neutral current (Z^0).[1] At typical operating energies of SLC[2] and LEP,[3] the interaction will be dominated through neutral current via Z^0-production. Furthermore, large enhancements in the value of cross section for $e^+e^- \rightarrow$ hadrons is expected at Z^0 resonance, i.e. at c.m. total energy of $\sqrt{s} \sim M_Z$. However, at lower energies, (i.e., $\sqrt{s} \sim 20$ GeV), the process is dominated by electromagnetic current and Z^0 contribution will be negligible. The interesting region of medium energy (e.g. TRISTAN[4] energies) will reveal the interference between weak and electromagnetic interactions.

Related to the variation of energy in inclusive hadron production, it is interesting to study the angular distribution of produced hadrons. At energies slightly above threshold, the reaction is almost like a two-body exclusive process. Therefore, the angular distribution is determined by the helicity of the final state hadrons. However, at higher energies, multiparticle production dominates and the spin correlations among produced hadrons become unimportant. In fact, at asymptotic high energies, the angular distribution of the hadron in inclusive reaction is basically determined by the quark-antiquark pair production.

Another interesting feature of angular distribution of hadrons comes from weak and electromagnetic interference.[1] The axial coupling of Z^0 boson to fermion gives rise to asymmetry in the angular distribution. This leads to forward-backward asymmetry which can provide valuable information about the coupling of Z^0 to quarks.

In this paper, we have studied the inclusive production of heavy mesons (mesons with at least one heavy quark c, b, t) for the energy ranges from 20 GeV to 110 GeV. From a theoretical point of view, heavy meson systems are interesting because: (i) their binding energies are small compared to their masses and therefore to a good approximation they are nonrelativistic systems described by simple wave functions (see next section), (ii) the momentum transfer q involved in the production of heavy quarks is sufficiently large compared to QCD scale parameter $\Lambda_{\rm QCD} \sim 100$ MeV. Thus, the heavy meson system could provide important clues related to the perturbative QCD mechanism for the hadronization process.[5]

This paper is organized as follows. In Section 2, we present the details of the calculation for production of heavy mesons. We derive analytic expressions for various cross sections at high energy limit in Section 3. The numerical estimates of total cross section, fragmentation function, angular distribution and asymmetry for pseudoscalar mesons are given in Section 4. A summary and conclusions are followed in Section 5.

2. Calculation of Cross Section

The mechanism for inclusive production of heavy mesons is shown in Fig. 1. In Figs. 1(a) and 1(b), the process is mediated via photon production while in Figs. 1(c) and 1(d) it is mediated through Z^0 boson. The main contribution from each set of diagrams depends on the energy regions as it was discussed in the Introduction.

At large momentum transfer q, the invariant amplitude M for processes shown in Fig. 1 factorizes[5,6] into the convolution of hard scattering amplitude T_H and meson distribution amplitude ϕ_M. Therefore, we can write M as,

$$M\left(k_i, q_i\right) = \int [dx]\; T_H\left(k_i, q_i, x_i\right)\; \phi_M\left(x_i, q^2\right) \tag{1}$$

where T_H is the hard scattering amplitude which can be calculated perturbatively from quark-gluon subprocesses, and ϕ_M is the probability amplitude to find quarks which are collinear up to the scale q^2 in a mesonic bound state. In Eq. (1), x_i's are the momentum fractions carried by constituent quarks and $[dx]= dx_1 dx_2 \delta(1 - x_1 - x_2)$. For the heavy quark systems, the bound state wave function can be reliably determined by nonrelativistic considerations.[6] Therefore, we use the quark distribution amplitude ϕ_M, given in Ref. 6 which is derived in the same approximation. For pseudoscalar mesons, ϕ_M is given by

$$\phi_M\left(x_i, q^2\right) = \frac{f_M}{2\sqrt{3}}\, \delta\left(x_1 - \frac{m_1}{m}\right) \tag{2}$$

where f_M is the pseudoscalar meson decay constant and m and m_1 are masses of the meson and the primary quark respectively. By substituting Eq. (2) into

Eq. (1), the invariant amplitude $\mathcal{M}$ becomes,

$$\mathcal{M}\left(k_i, q_i\right) = \frac{f_M}{2\sqrt{3}}\, T_H\left(k_i, q_i, r\right) \tag{3}$$

where $r = m_1/m$. Using the spin sum,[7]

$$\frac{1}{\sqrt{2}} \sum_{\text{spin}} v(p)\ \bar{u}(p) = \frac{\gamma_5(\not{p} + m)}{\sqrt{2}} \quad , \tag{4}$$

for pseudoscalar mesons, the hard scattering amplitude T_H can be expressed as

$$\begin{aligned} T_H = \sum_{I=\gamma, Z^0} & i\, \frac{16\pi^2 C_F \alpha \alpha_s}{(1-r)s(\sqrt{s} - 2E_1)s_I}\, \bar{v}(k_2)\gamma^\mu\, \Gamma_e^I\, u(k_1) \\ & \times \left\{ \frac{\bar{u}(q_2)\gamma_\alpha\, \frac{\gamma_5(\not{p}+m)}{\sqrt{2}}\, \gamma^\alpha(\not{p} + \not{q}_2 + rm)\gamma_\mu\, \Gamma_Q^I\, v(q_1)}{\sqrt{s} - 2E_1} \right. \\ & \left. + \frac{\bar{u}(q_2)\gamma_\alpha\, \frac{\gamma_5(\not{p}+m)}{\sqrt{2}}\, \gamma_\mu\, \Gamma_Q^I \{-[\not{q}_1 + \not{q}_2 + (1-r)\not{p}] + rm\}\gamma^\alpha\, v(q_1)}{\sqrt{s} - 2rE} \right\} \\ & + (\text{primary} \leftrightarrow \text{secondary}) \end{aligned} \tag{5}$$

where

$$\begin{aligned} s_\gamma &= s \quad , & s_{Z^0} &= 4\sin^2 2\theta_W \left(s - M_Z^2 + i\Gamma_Z M_Z\right) \\ \Gamma_e^\gamma &= -1 \quad , & \Gamma_e^Z &= V_e + A_e\, \gamma_5 \\ \Gamma_Q^\gamma &= Q \quad , & \Gamma_Q^Z &= V_Q + A_Q\, \gamma_5 \end{aligned} \tag{6}$$

with

$$\begin{aligned} V_Q &= 2I_3 - 4Q\sin^2\theta_W \quad , \quad V_e = 4\sin^2\theta_W - 1 \\ A_Q &= -2I_3 \quad , \quad A_e = 1 \quad . \end{aligned} \tag{7}$$

Here I_3 is the third component of the weak isospin of the quark coupled to Z^0 and Q is the charge of the quark. In Eq. (5), α is the fine structure constant,

the color factor $C_F = 4/3$, E and E_1 are energies of the meson and the primary quark respectively, and (primary $\leftrightarrow$ secondary) indicates the contributions from the diagrams in which primary quark pair is exchanged with secondary quark pair.

Now the square of the invariant amplitude $\mathcal{M}$ becomes

$$|\mathcal{M}|^2 = \frac{f_M^2}{12} \frac{128\pi^4 C_F^2 \alpha^2 \alpha_s^2}{(1-r)^2 s^2 (\sqrt{s} - 2E_1)^2} \sum_{I,J}^{\gamma, Z^0} \frac{1}{s_I s_J^*} L^{\mu\nu}(I,J)\, H_{\mu\nu}(I,J) \ , \qquad (8)$$

where

$$L^{\mu\nu}(I,J) = \mathrm{Tr}\left(\not{k}_2 \gamma^\mu \Gamma_e^I \not{k}_1 \widetilde{\Gamma}_e^J \gamma^\nu \right) \qquad (9)$$

and

$$\begin{aligned}
H_{\mu\nu}(I,J) = & -\frac{4}{(\sqrt{s}-2E_1)^2} \mathrm{Tr}\Big\{ [\not{q}_2 + (1-r)m]\, \gamma_5 (\not{p} - 2m)(\not{p} + \not{q}_2 + rm) \\
& \times \gamma_\mu \Gamma_Q^I (\not{q}_1 - rm) \widetilde{\Gamma}_Q^J \gamma_\nu (\not{p} + \not{q}_2 + rm)(\not{p} - 2m)\gamma_5 \Big\} \\
& + \frac{4}{(\sqrt{s}-2E_1)(\sqrt{s}-2rE)} \mathrm{Re}\Big\{ \mathrm{Tr}\{ [\not{q}_2 + (1-r)m] \\
& \times \gamma_5 (\not{p} - 2m)(\not{p} + \not{q}_2 + rm) \gamma_\mu \Gamma_Q^I (\not{q}_1 - rm) \\
& \times \gamma^\alpha (\not{q}_1 + \not{q}_2 + (1-r)\not{p} - rm) \widetilde{\Gamma}_Q^J \gamma_\nu (\not{p} + m) \gamma_5 \gamma_\alpha \} \Big\} \\
& - \frac{1}{(\sqrt{s}-2rE)^2} \mathrm{Tr}\Big\{ [\not{q}_2 + (1-r)m] \gamma_\alpha \gamma_5 (\not{p} + m) \\
& \times \gamma_\mu \Gamma_Q^I (\not{q}_1 + \not{q}_2 + (1-r)\not{p} - rm) \gamma^\alpha (\not{q}_1 - rm) \\
& \times \gamma^\beta (\not{q}_1 + \not{q}_2 + (1-r)\not{p} - rm) \widetilde{\Gamma}_Q^J \gamma_\nu (\not{p} + m) \gamma_5 \gamma_\beta \Big\} \ . \qquad (10)
\end{aligned}$$

In Eqs. (9) and (10), $\widetilde{\Gamma}_a \equiv V_a - \gamma_5 A_a$. Using Eqs. (8)-(10), we can calculate the differential cross section for the process $e^+e^- \to \text{meson} + X$:

$$d\sigma = \frac{|\bar{\mathcal{M}}|^2}{2s} \frac{d^3p}{2E} \frac{d^3q_1}{2E_1} \frac{d^3q_2}{2E_2} \frac{1}{(2\pi)^5} \delta^4(k_1 + k_2 - p - q_1 - q_2) \tag{11}$$

where $|\bar{\mathcal{M}}|^2$ is the square of the spin averaged invariant amplitude. Utilizing energy momentum conservation, the differential cross section (11) becomes,

$$\begin{aligned} d\sigma = {} & \frac{|\bar{\mathcal{M}}|^2}{64(2\pi)^5} \, dz \, dy \, d\cos\theta \, d\phi \, d\cos\theta_{MQ} \, d\phi_{MQ} \\ & \times \delta\left(\cos\theta_{MQ} - \frac{2 - 2(y+z) + yz + r\tau^2}{\sqrt{z^2 - \tau^2}\,\sqrt{y^2 - r^2\tau^2}}\right) \theta(2 - y - z) \end{aligned} \tag{12}$$

where $y = 2E_1/\sqrt{s}$, $z = 2E/\sqrt{s}$, $\tau^2 = 4m^2/s$, angles (θ, ϕ) specify the direction of the meson with respect to the beam axis, (θ_{MQ}, ϕ_{MQ}) determine the direction of the primary quark with respect to the meson and the function $\theta(2 - y - z)$ is theta function. The final form of the differential cross section can be obtained by integrating over $\cos\theta_{MQ}$ and ϕ (integrand is independent of azimuthal angle of the meson). Therefore, we get

$$d\sigma = \frac{|\bar{\mathcal{M}}|^2}{1024\pi^4} \, dz \, dy \, d\cos\theta \, d\phi_{MQ} \quad . \tag{13}$$

The limits of y integration[5] satisfy the equation $\cos^2\theta_{MQ} = 1$, or

$$\{4(1-z)+\tau^2\}y^2 - 2(2-z)\{2(1-z)+r\tau^2\}y + \{2(1-z)+r\tau^2\}^2 + r^2\tau^2(z^2-\tau^2) = 0 \quad . \tag{14}$$

In the following section, we will use Eqs. (8)-(13) to determine cross sections for various pseudoscalar mesons.

3. Cross Sections at High Energy Limit

In this section we derive an analytic expression for the differential cross section of Eq. (13) in the limiting case of $m^2/s \to 0$. This high energy limit is mainly applicable to the production of D and B mesons at SLC and LEP energies where meson mass can be neglected compare to total c.m. energy.

Let's return to Eq. (14) where its solutions represent the limits of y-integration in differential cross section of Eq. (13). If $\tau^2 = 4m^2/s \ll 1$, then the solutions[5] of Eq. (14) to the first order of τ^2 are

$$\begin{aligned} y_\ell &= 1 - z + \frac{\{1-(1-r)z\}^2}{4z(1-z)}\,\tau^2 \\ y_u &= 1 - \frac{\{1-(1-r)z\}^2}{4z(1-z)}\,\tau^2 \quad . \end{aligned} \tag{15}$$

Consequently, by integrating over y and using the limits given by (15), the differential cross section becomes,

$$\begin{aligned} \lim_{\tau^2\to 0}\frac{d\sigma}{dz} = {} & \frac{2\pi\alpha^2\alpha_s^2 f_M^2}{27\sin^4 2\theta_W m^2}\,\frac{s}{\{(s-M_Z^2)^2+\Gamma_Z^2 M_Z^2\}} \\ & \times z(1-z)^2\left[\Gamma_p\,\frac{\{1+(1-r)z\}^2}{(1-r)^2(1-rz)^4} + \Gamma_s\,\frac{(1+rz)^2}{r^2\{1-(1-r)z\}^4}\right] \end{aligned} \tag{16}$$

where

$$\Gamma_{p,s} = \frac{1}{3}\left(V_{p,s}^2 + V_{Qp,s}^2 A_e^2 + A_{Qp,s}^2 V_e^2 + A_{Qp,s}^2 A_e^2\right) \tag{17}$$

with

$$V_{p,s} = V_{Qp,s}V_e - 4Q_{p,s}\sin^2 2\theta_W\,\frac{(s-M_Z^2)^2+\Gamma_Z^2 M_Z^2}{s^2} \quad . \tag{18}$$

Here $Q_{p,s}$ refer to primary and secondary quark charges. Now we calculate the fragmentation function $D_Q^M(z)$ which is related to the differential cross section

by

$$D_Q^M(z) \equiv \frac{1}{\sigma}\,\frac{d\sigma}{dz} \quad , \tag{19}$$

where σ is the total cross section and is obtained by integrating Eq. (16). The result is,

$$\sigma = \frac{2\pi\alpha^2\alpha_s^2 f_M^2}{27\sin^4 2\theta_W m^2}\,\frac{s}{\{(s-M_Z^2)^2+\Gamma_Z^2 M_Z^2\}}\,\{\Gamma_p\, g(r)+\Gamma_s\, g(1-r)\} \tag{20}$$

where

$$\begin{aligned} g(r) = {} & \frac{\ln(1-r)}{r^6(1-r)^2}\,(10-20r+16r^2-6r^3+r^4) \\ & + \frac{1}{6r^5(1-r)^3}\,(60-150r+146r^2-69r^3+15r^4) \quad . \end{aligned} \tag{21}$$

Therefore using Eqs. (16) and (20), the fragmentation function defined by (19) becomes,

$$\begin{aligned} D_Q^M(z) = {} & z(1-z)^2\left[\Gamma_p\,\frac{\{1+(1-r)z\}^2}{(1-r)^2(1-rz)^4}+\Gamma_s\,\frac{(1+rz)^2}{r^2\{1-(1-r)z\}^4}\right] \\ & \Big/\Big\{\Gamma_p\, g(r)+\Gamma_s\, g(1-r)\Big\} \end{aligned} \tag{22}$$

where $\Gamma_{p,s}$ is given by Eq. (17).

It is interesting to note that even though experimental data from SLC or LEP are not yet available, but the measurements of fragmentation functions of heavy quarks at PEP or PETRA indicate $(1-z)^2$ behavior at large z values, i.e. z close to 1. This is precisely what is predicted by Eq. (22). Furthermore, at r values near 1, e.g. for D and B mesons, the contributions from secondary quark

pair (light quark-antiquark pair) in Eqs. (16) and (20) become negligible and we get

$$D_Q^M(z) \approx \frac{1}{g(r)} \frac{\{1+(1-rz)\}^2}{(1-r)^2(1-rz)^4} z(1-z)^2 \quad , \tag{23}$$

where $g(r)$ is given by (21). Therefore, the coefficient Γ_p which contain the information about the coupling of Z^0 to quarks and leptons cancel and the fragmentation function become exactly what was calculated in Ref. 5 based on only photon exchange . The fragmentation function as given by Eq. (23) peaks[8] at $z_{\rm peak} \approx 1/\sqrt{5-5r+r^2}$. For D mesons $z_{\rm peak} \approx 0.8$ while for B mesons $z_{\rm peak} \approx 0.9$. For T mesons $(t\bar{u})$, $z_{\rm peak}$ appears very close to 1 and the fragmentation function behaves like a delta function.

The analytic expressions for angular distribution of produced mesons can be calculated using the same technique. The result is summarized as

$$\begin{aligned} \frac{d\sigma}{d\cos\theta} = & \frac{\alpha^2\alpha_s^2 f_M^2}{\sin^4 2\theta_W\{(s-M_Z^2)^2+\Gamma_Z^2 M_Z^2\}s^3 m^2} \\ & \times \left[\frac{F_p}{(1-r)^2} + (\text{primary} \leftrightarrow \text{secondary})\right] \quad , \end{aligned} \tag{24}$$

where F_p is a function which has the general form of

$$F_p = C_0 + C_1\cos\theta + C_2\cos^2\theta \quad . \tag{25}$$

The coefficients C_i's are functions of r and couplings V_Q, A_Q, etc. The exact form of F_p will not be presented here because of lengthy expression, however, the predictions of Eq. (24) will be examined in the next section.

4. Numerical Estimates

In this section, we present the numerical estimates of (a) total cross section, (b) fragmentation function, (c) angular distribution and (d) forward-backward asymmetry. As can be seen from Eq. (8), there are several factors for which there are no accurate experimental data. For example, the meson decay constant f_M is not known for all cases we are considering. In our numerical results we used the following values:

$$\begin{array}{lll} \alpha_s = 0.2 & f_M = 0.28 \text{ GeV} & \Gamma_Z = 2.9 \text{ GeV} \\ m_t = 40 \text{ GeV} & m_b = 5 \text{ GeV} & m_c = 1.5 \text{ GeV} \\ m_u = 0.3 \text{ GeV} & M_Z = 92.9 \text{ GeV} & \sin^2\theta_W = 0.23 \quad . \end{array} \tag{26}$$

(a) Total Cross Section

For D and B mesons, total cross section at high c.m. energies ($\sqrt{s} \gtrsim 60$ GeV) is given by the analytic result of Eq. (20). The contributions due to higher twist mass effects are not very large and we found these corrections are about 20%-30% [see Sections 4(b) and 4(c)]. However, for T mesons, the higher twist mass effects cannot be neglected because τ^2 is no longer small. Consequently, in this case all mass terms must be included in the predictions.

The total cross sections for D and B mesons, as predicted by Eq. (20), are shown in Figs. 2(a) and 2(b). At Z^0 pole, i.e. $\sqrt{s} = 92.9$ GeV, the total cross section peaks and increases by approximately two orders of magnitude compared to $\sqrt{s} = 60$ GeV. The fact that the cross sections in Figs. 2(a) and 2(b) are not decreasing around $\sqrt{s} = 60$ GeV is due to the contributions from Z^0 exchange. This effect should be observable at TRISTAN energies. For lower energies, this contribution becomes smaller as compared to higher energy cases. Therefore,

photon exchange dominates and the cross section decreases as $1/s$. This $1/s$ behavior is also recovered once the energy $\sqrt{s} \gg M_Z$. In Fig. 2(c) we have shown the total cross section of T meson which includes all mass terms. In this calculations we used the algebraic manipulation program REDUCE and the Monte Carlo integration routine VEGAS.[9] As we see from Fig. 2(c), at Z^0 pole the $T(t\bar{u})$ meson total cross section is approximately the same order of magnitude as $B(b\bar{u})$ and $D(c\bar{u})$ mesons. Consequently, we expect a large contribution from T meson in direct hadronic production channels at SLC and LEP.

(b) Fragmentation Function

Since the fragmentation function is defined by the ratio of two cross sections i.e. $D(z) \equiv (1/\sigma)d\sigma/dz$, the corrections due to higher twist mass effects are negligible. The leading twist calculation of fragmentation function was presented in Section 3 where we derived an analytic expression for $D(z)$ given by Eq. (22). As we mentioned in Section 3, for r close to 1, the fragmentation function is independent of the nature of exchanged particle (i.e. γ, Z^0 or both) and is only a function of z. In Figs. 3(a) and 3(b) we have compared the predictions of Eq. (22) with the experimental data.[10] They are in reasonable agreement with the data for c and b quark fragmentation functions. These calculations can be easily extended to vector mesons[5] and the results are shown by dashed curves in Figs. 3(a) and 3(b). For family of T mesons ($t\bar{u}$, $t\bar{s}$, etc.), the value of r is very close to 1 and due to mass threshold, the expected kinematic range of z for $D_Q^M(z)$ is quite reduced to $z \approx 1$. In fact to a good approximation, it can be considered as $D_Q^M(z) \sim \delta(z - z_{\text{peak}})$, where is z_{peak} is nearly 1.

The differential cross section $d\sigma/dz$ for B mesons is shown in Fig. 4. The solid line represents the calculations with all the mass terms included, while the

dashed line is the prediction of the analytic expression (16). From Fig. 4, it is observed that higher twist mass effects in average account for corrections of approximately 20%-30%.

(c) Angular Distribution

At low energies (e.g. $\sqrt{s} \approx 20$ GeV), the angular distribution of B mesons is expected to have a general form like $a + b\cos^2\theta$. In other words, at these energy ranges the contributions from axial vector coupling due to Z^0 exchange is negligible and the angular distribution is symmetric. As energy increases, the axial vector coupling makes larger contributions and the angular distribution gradually becomes asymmetric and behaves like $A + B\cos\theta + C\cos^2\theta$ [see Eq. (24)]. This property is clearly shown in Figs. 5 and 6 where we have plotted angular distributions of B and T mesons at various c.m. energies. As we see from Fig. 5(a), the angular distribution of B meson at $\sqrt{s} = 11$ GeV is almost flat (notice the scale). In fact, near threshold, the process is dominated by two body exclusive production and the angular distribution is effected by the spin correlations between the two produced mesons. Since we require one of the produced mesons to be a pseudoscalar, the other meson is most likely a pseudoscalar or a vector. Therefore, the net angular distribution, which is a combination[11] of $\sin^2\theta$ (pseudoscalar-pseudoscalar) and $1 + \cos^2\theta$ (pseudoscalar-vector), shows very small variation in the entire range of $\cos\theta$. This threshold behavior is also observed for T meson production as shown in Fig. 6(a). However, as energy increases, angular distributions become more concave because multiparticle channels give larger contributions. This behavior is observed in both Figs. 5 and 6 for B and T mesons respectively.

(d) Forward-Backward Asymmetry

As we discussed in Section 4(c), the interference between vector and axial vector currents gives rise to asymmetry in angular distributions at high energies. This interference arise from γ and Z^0 cross diagrams or from the product of vector and axial coupling terms in Z^0 diagram alone. The latter contribution is generally negligible due to the very small magnitude of the vector coupling of Z^0 to leptons. Therefore, the main contribution to the asymmetry is coming from weak-electromagnetic interference terms.

To measure asymmetry, the forward-backward asymmetry A_{FB} is defined as

$$A_{FB} = \frac{1}{\sigma}\left(\int_0^1 \frac{d\sigma}{d\cos\theta}\, d\cos\theta - \int_{-1}^0 \frac{d\sigma}{d\cos\theta}\, d\cos\theta\right) \quad . \tag{27}$$

The asymmetries for D, B and T mesons are shown in Figs. 7 and 8. Since the photon diagram is dominant at low energies, the asymmetry is very small near the threshold of D and B meson production (see Fig. 7). However, for $50 \lesssim \sqrt{s}/\mathrm{GeV} \lesssim 80$, the interference between γ and Z^0 gives a significant contribution to the process. Consequently, at TRISTAN energies, the asymmetry expected to be large. At Z^0 pole, the photon contribution is negligible and as a result the asymmetry becomes very small. For higher energies, photon contributions cannot be neglected. In fact, the asymmetry reaches a constant value at asymptotic high energies ($\sqrt{s} \gg M_Z$).

One of the interesting features of Figs. 7 and 8 is the mass effect. Comparing these figures, we note that the form of the asymmetry of the T mesons around Z^0 pole is quite different from that of D and B mesons. This is basically due to the large t quark mass compare to c and b quarks, which causes the higher

twist mass effects to be much more significant for T mesons than D or B mesons. The same behavior can also be observed in the angular distribution of B and T mesons (see Figs. 5 and 6).

5. Conclusions

In the preceding sections we analyzed the inclusive production of pseudoscalar heavy mesons in e^+e^- annihilation. For D and B meson production, the higher twist mass effects give 20% -30% corrections at total c.m. energy of about 60 GeV. Even at $\sqrt{s} \sim 20$ GeV, these corrections are still less than 50%. On the other hand, for T meson production, these effects are quite significant within the energy range we are considering and must be included in the analysis.

Our predictions for the normalization of the cross sections depend on parameters which are not yet well determined. However, the predictions for fragmentation functions and forward-backward asymmetry are relatively independent of uncertain input parameters. The analytic expression (22) for the heavy quark fragmentation function gives a reasonable agreement with the experimental data for D and B mesons. The measurement of the forward-backward asymmetry at energies slightly below Z^0 production will provide a good opportunity to test the prediction of higher twist mass effects in T meson production, as well as the interference between weak and electromagnetic currents.

Acknowledgements

We are indebted to Stan Brodsky for suggesting to include weak-electromagnetic interference in this paper and useful discussions throughout this work. We also wish to thank Ben Harms for helpful suggestions at the early stage of this work and Ken Aoki for illuminating conversations. One of us (F.A.) would like to thank SLAC for hospitality during the completion of this project.

References

1. C. Quigg, *Gauge Theories of the Strong, Weak, and Electromagnetic Interactions*, The Benjamin Cummings Publishing Co., 1983.
2. Proceedings of the SLC Workshop on Experimental Use of the SLAC Linear Collider, SLAC Report 247, 1982.
3. *Physics at LEP*, Ed. by John Ellis and Roberto Pecei, CERN 86-02, 1986.
4. Proceedings of the second TRISTAN Physics Workshop, Ed. Y. Unno, KEK 82-1, 1982.
5. F. Amiri and C.R. Ji, SLAC-PUB-4023, 1986 (submitted to Phys. Rev. Lett.).
6. G.P. Lepage and S.J. Brodsky, Phys. Rev. **D22**, 2157 (1980); S.J. Brodsky and C.R. Ji, Phys. Rev. Lett. **55**, 2257 (1985); F. Amiri, B.C. Harms and C.R. Ji, Phys. Rev. **D32**, 2982 (1985).
7. E.L. Berger and D. Jones, Phys. Rev. **D23**, 1521 (1981).
8. By minimizing the momentum transfer carried by gluon in Fig. 1, one can derive $z_{\rm peak}$ up to the order of r^2 as $z_{\rm peak} = \frac{1}{2-r}[1+r^2(1-r)]$; see L. Clavelli, Phys. Rev. **D26**, 1610 (1982).
9. G.P. Lepage, J. Comp. Phys. **27**, 192 (1978).
10. J. Chapman, in Proceedings of 1984 SLAC Summer Institute, Stanford, California; J. Dorfan, in International Symposium on Lepton and Photon Interactions at High Energy, Ithaca, New York, 1983; B. Adeva *et al.*, Phys. Report **109**, 121 (1984).
11. See S.J. Brodsky and C.R. Ji in Ref. 6.

Figure Captions

Fig. 1. Inclusive production of mesons in e^+e^- annihilations. Four more diagrams can be obtained by exchanging primary and secondary quark pairs.

Fig. 2. Total cross sections for inclusive production of (a) D meson, (b) B meson, and (c) T meson.

Fig. 3. (a) Charm and (b) Bottom fragmentation predictions Eq. (22), compared to various experimental data.[10] The solid curves in (a) and (b) are pseudoscalar mesons and the dashed curves are vector mesons.

Fig. 4. Differential cross section for B meson at $\sqrt{s} = 50$ GeV. The dashed curve is the prediction of Eq. (20) and the solid curve is the numerical estimate which includes higher twist mass effects.

Fig. 5. Angular distribution of B $(b\bar{u})$ meson at (a) $\sqrt{s} = 11$ GeV, (b) $\sqrt{s} = 29$ GeV, (c) $\sqrt{s} = 60$ GeV, (d) $\sqrt{s} = 80$ GeV, (e) $\sqrt{s} = 90$ GeV. The solid curves in (a), (b) and (c) are the numerical estimates with higher twist mass effects. The dashed curve in (c) and the solid curves in (d) and (e) are predictions of Eq. (24).

Fig. 6. Angular distribution of T $(t\bar{u})$ meson at (a) $\sqrt{s} = 85$ GeV, and (b) $\sqrt{s} = 92.9$ GeV with higher twist mass effects.

Fig. 7. Forward-backward asymmetry for inclusive D and B meson productions.

Fig. 8. Forward-backward asymmetry for inclusive T meson production.

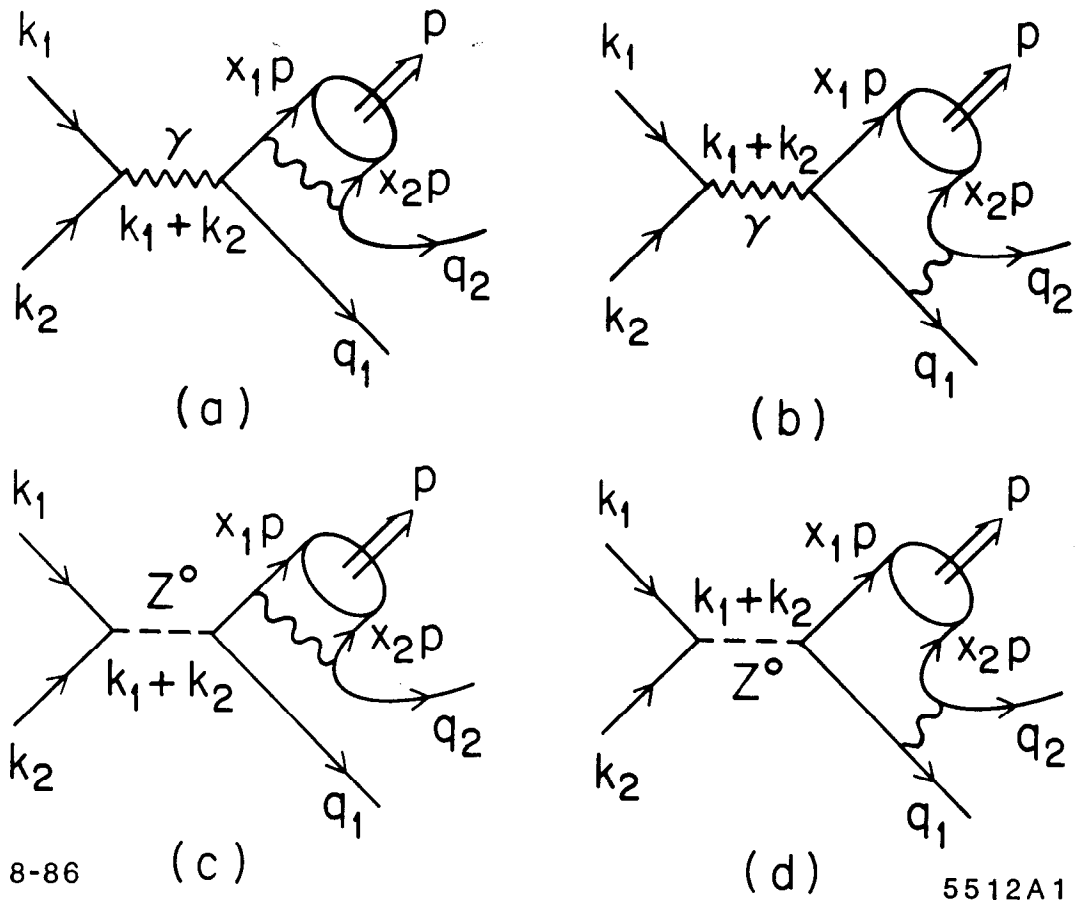
k1
k2
γ
k1 + k2
x1p
x2p
p
q1
q2
(a)
k1
k2
k1 + k2
γ
x1 p
x2p
p
q1
q2
(b)
k1
k2
Z°
k1 + k2
x1p
x2p
p
q1
q2
(c)
k1
k2
k1+k2
Z°
x1 p
x2p
p
q1
q2
(d)
8-86
5512A1

Fig. 1

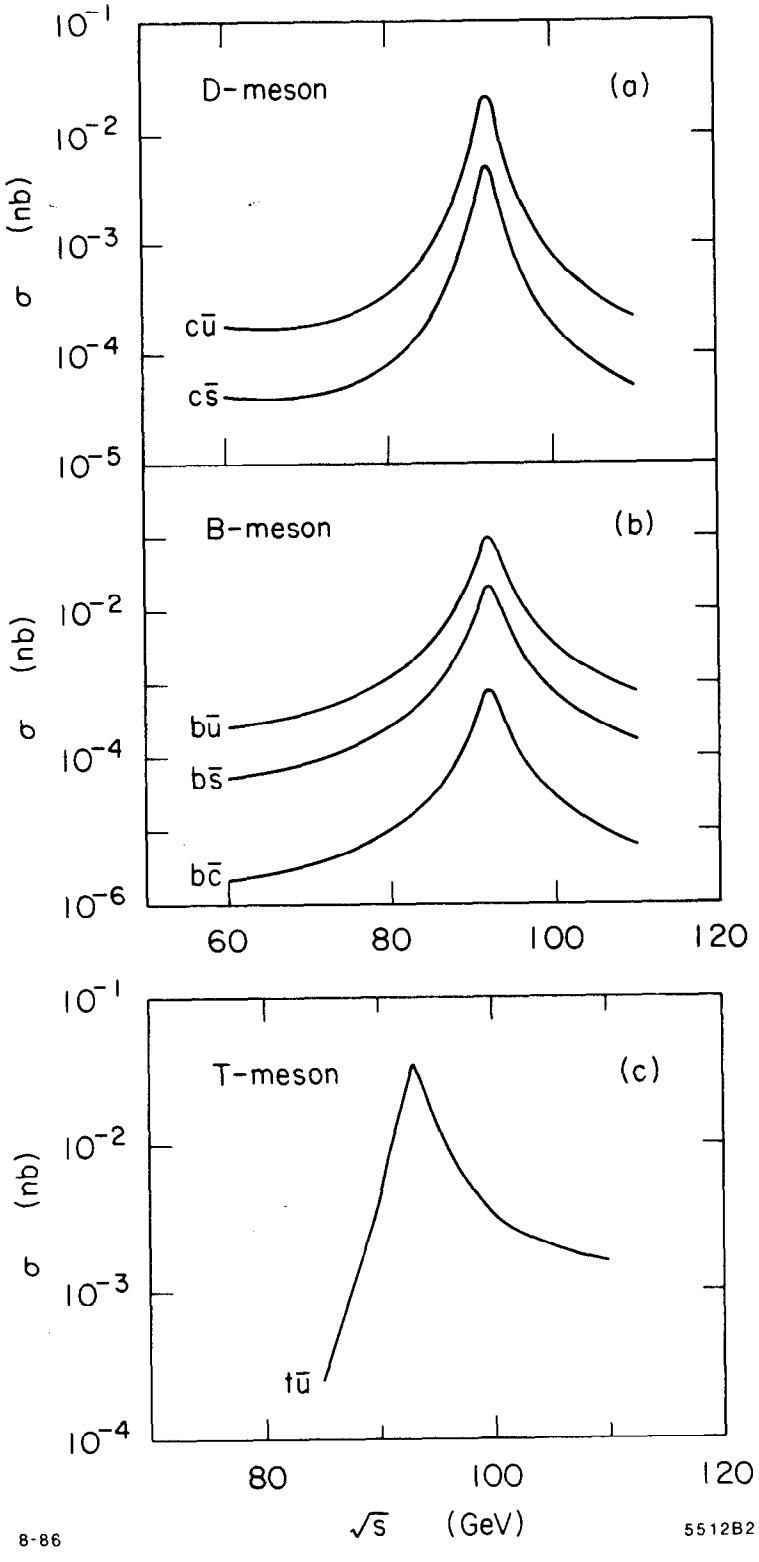
D-meson
(a)
cū
cs̄
B-meson
(b)
bū
bs̄
bc̄
T-meson
(c)
tū
σ (nb)
10^-1
10^-2
10^-3
10^-4
10^-5
10^-6
60
80
100
120
√s (GeV)
8-86
5512B2

Fig. 2

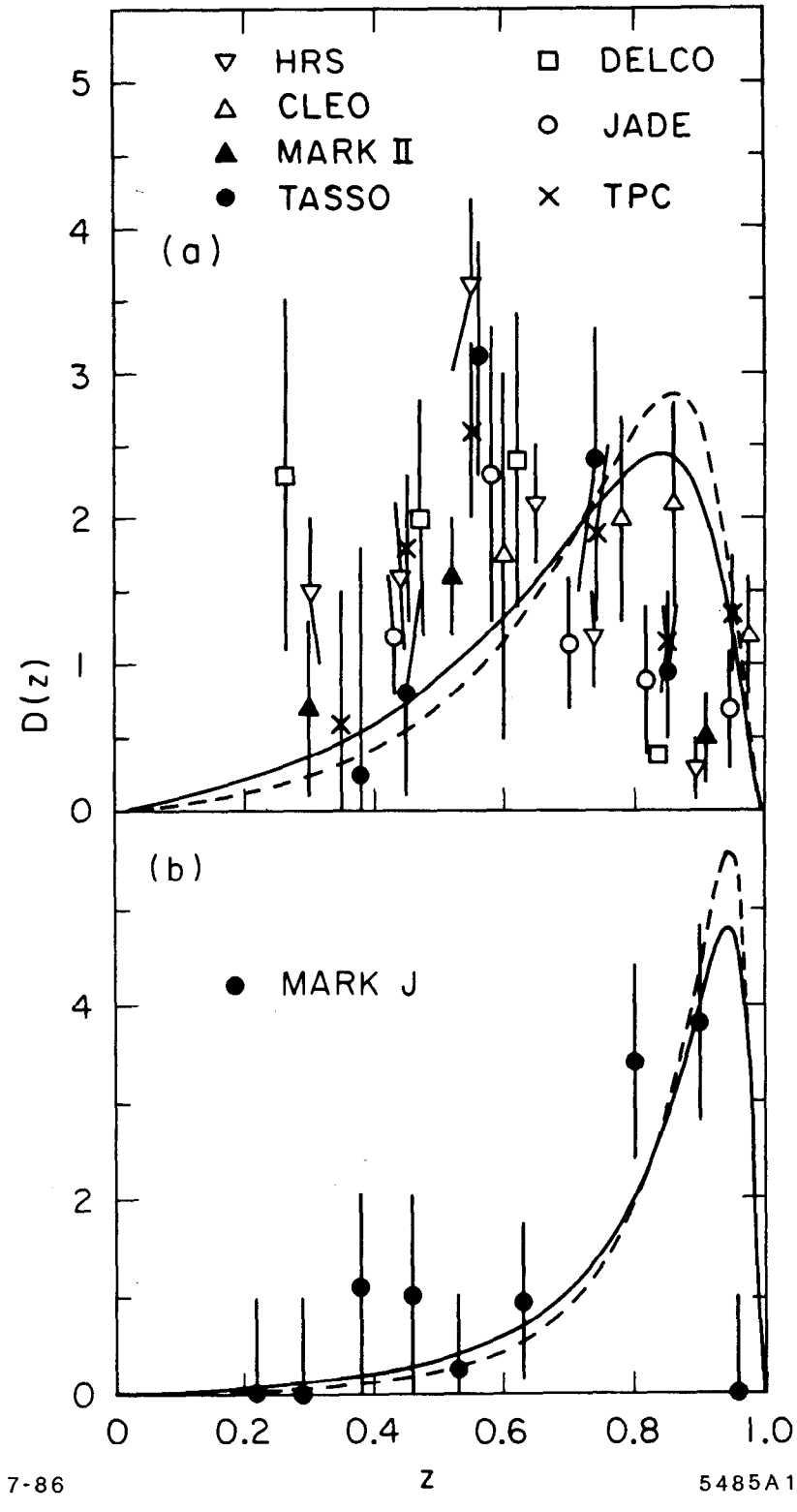
HRS
CLEO
MARK II
TASSO
DELCO
JADE
TPC
(a)
(b)
MARK J
D(z)
z
0
0.2
0.4
0.6
0.8
1.0
1
2
3
4
5
7-86
5485A1

Fig. 3

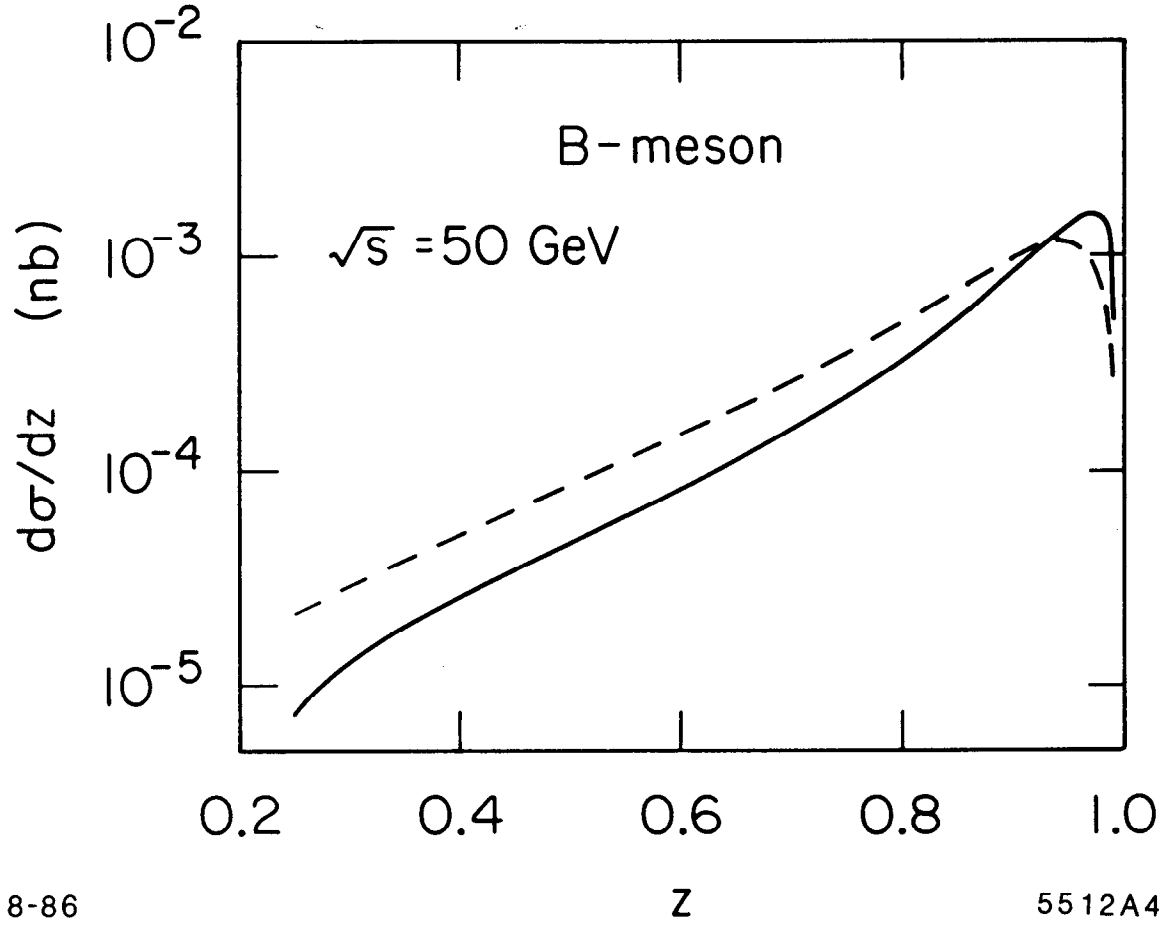
10^{-2}
10^{-3}
10^{-4}
10^{-5}
B-meson
$\sqrt{s}$ =50 GeV
$d\sigma/dz$ (nb)
0.2
0.4
0.6
0.8
1.0
Z
8-86
5512A4

Fig. 4

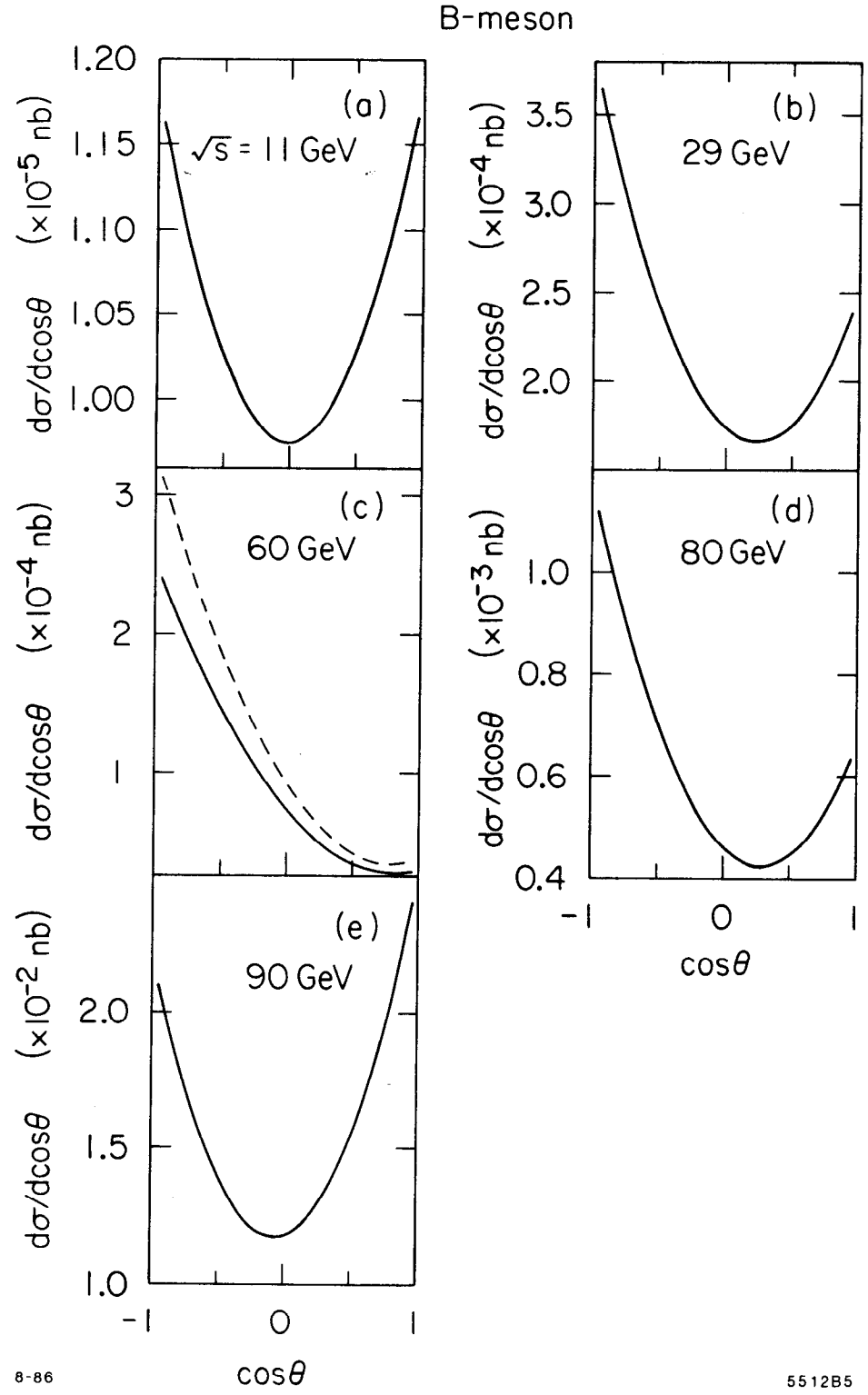
B-meson
(a)
√s = 11 GeV
(b)
29 GeV
(c)
60 GeV
(d)
80 GeV
(e)
90 GeV
dσ/dcosθ (×10⁻⁵ nb)
dσ/dcosθ (×10⁻⁴ nb)
dσ/dcosθ (×10⁻³ nb)
dσ/dcosθ (×10⁻² nb)
cosθ
8-86
5512B5

Fig. 5

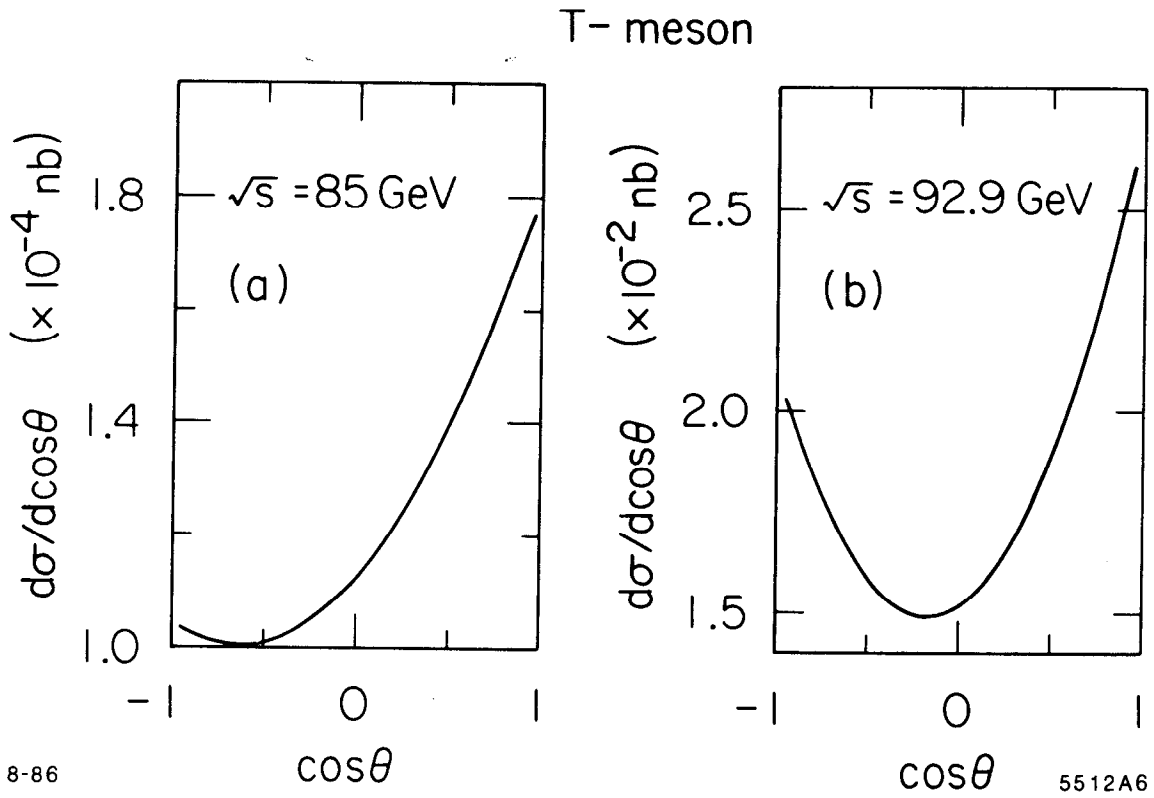
T- meson
√s = 85 GeV
(a)
dσ/dcosθ (× 10⁻⁴ nb)
1.8
1.4
1.0
-1
0
1
cosθ
8-86
√s = 92.9 GeV
(b)
dσ/dcosθ (×10⁻² nb)
2.5
2.0
1.5
-1
0
1
cosθ
5512A6

Fig. 6

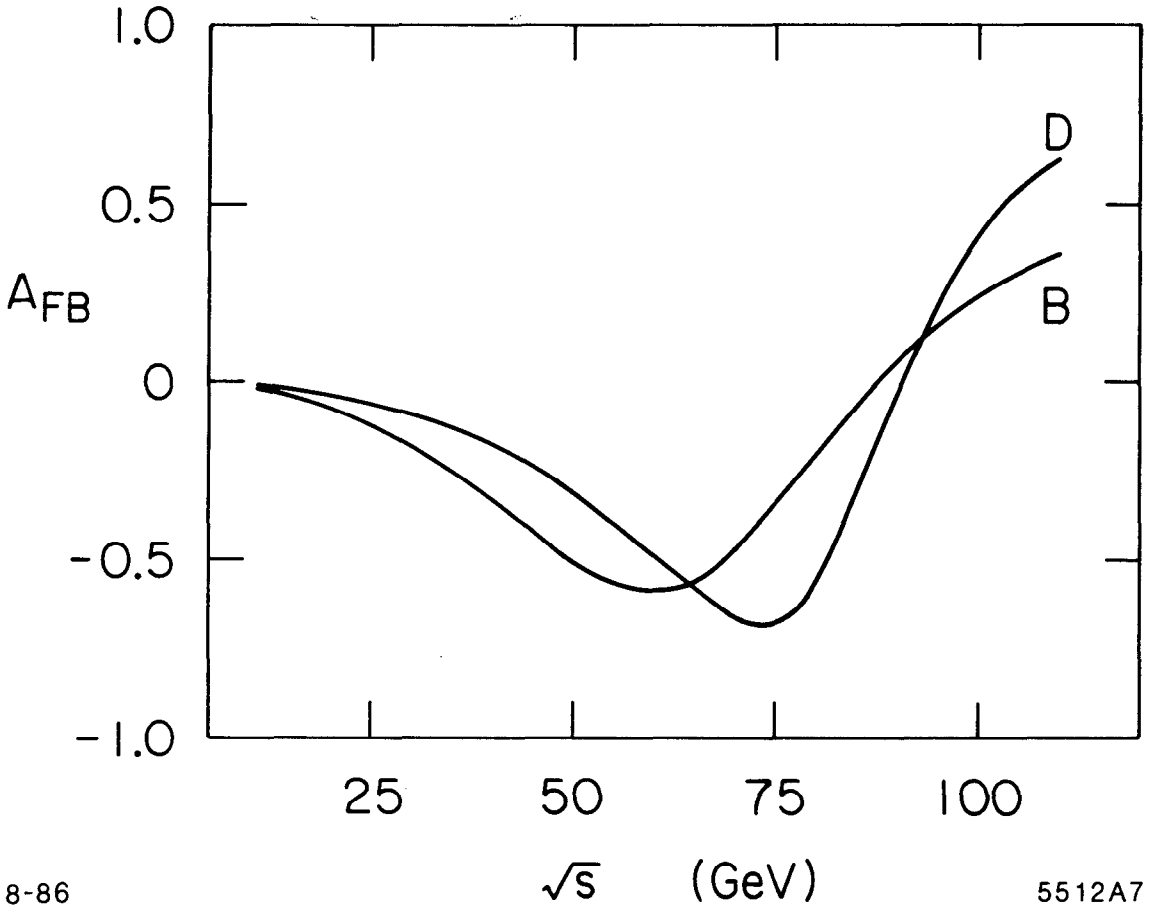

Fig. 7

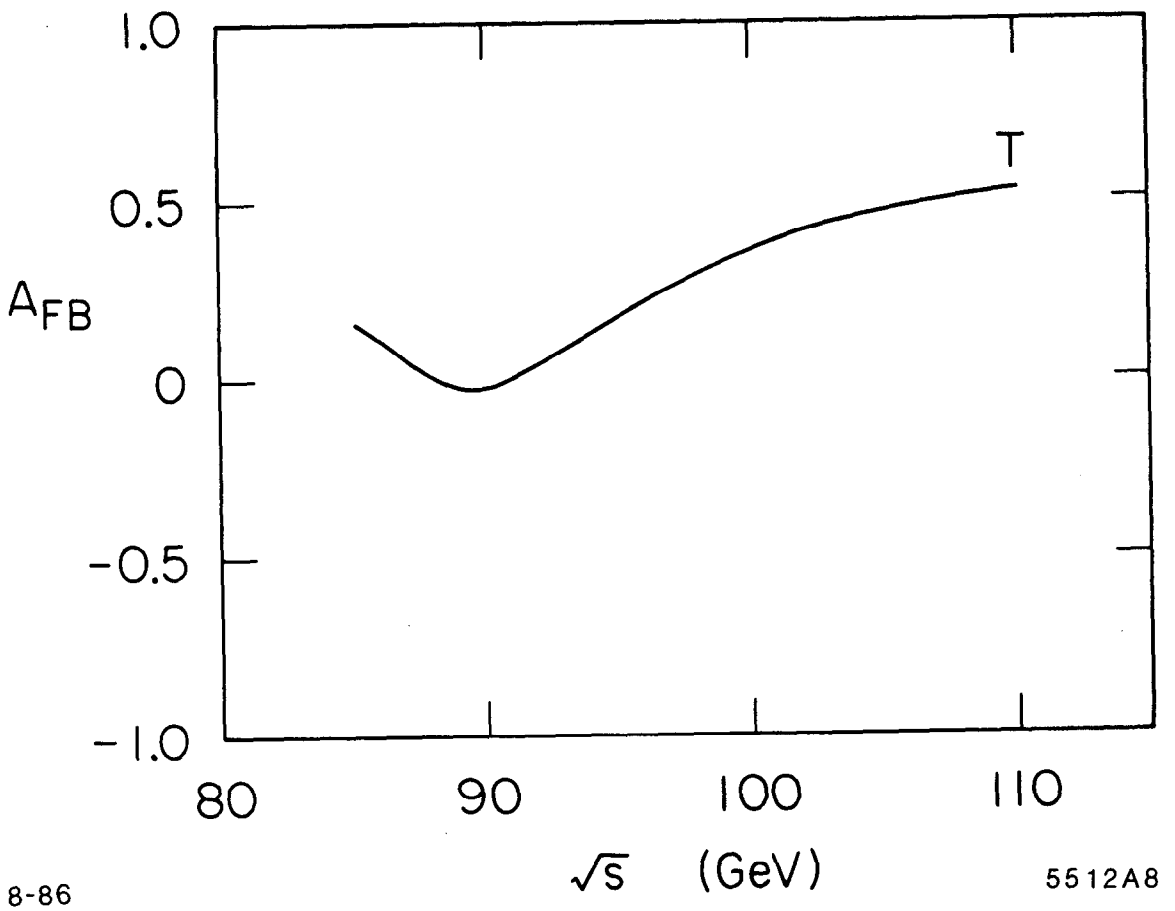

Fig. 8